Composite Structures 261 (2021) 113327

Contents lists available at ScienceDirect

Composite Structures

journal homepage: www.elsevier.com/locate/compstruct

Influence of layup, stacking sequence and loading rate on energy absorption of tension-absorber joints

Jazib Hassan [a,b], Ronan M. O'Higgins [a,b], Thomas Feser [c], Matthias Waimer [c], Conor T. McCarthy [a,b], Nathalie Toso [c], Michael A. McCarthy [a,*]

[a] Bernal Institute, School of Engineering, University of Limerick, Ireland
[b] CONFIRM Centre, University of Limerick, Ireland
[c] German Aerospace Center (DLR), Institute of Structures and Design, Stuttgart, Germany

ARTICLE INFO

Keywords:
Composite bolted joints
Energy absorption
Stacking sequence
Micro CT analysis

ABSTRACT

"Tension-absorber" joints are bolted joints designed to absorb energy in a survivable crash landing, through an extended version of bearing failure. They have been proposed for use in future transport aircraft narrow-body composite fuselages. Herein, the influence of layup (percentage of each ply orientation), stacking sequence (exact location of each ply) and loading rate, on energy absorption is examined. Quasi-static and dynamic (3 m/s) tests are performed on pin-loaded IM7/8552 carbon-fibre/epoxy laminates. Seven layups and 11 stacking sequences are tested, with key variables being the percentage of 0° plies (from 12.5% to 62.5%), the position of the 0° plies, and the changes in orientation at ply interfaces. Performance measures include ultimate bearing strength (UBS), mass-specific energy absorption (SEA) and crush load efficiency (CLE). Computed tomography is used to examine damage progression in the quasi-static tests. It is found that the most important factor in maximising SEA is having small changes in orientation at ply interfaces. This is even more important than 0° content. A laminate with only 12.5% 0° plies, performed remarkably well due to its low changes in ply orientation. Laminates with a high SEA tend to have a low UBS. Highest UBS was for quasi-isotropic laminates. Increased loading rate results in increased UBS but decreased SEA. The results allow selection of a stacking sequence with a desired combination of UBS and SEA, and provide a valuable database for validation of composites damage models.

1. Introduction

Mechanically fastened joints are widely used in composite aircraft structures. Recently [1,2], DLR and Airbus investigated using joints as energy-absorbing devices in future narrow-body composite aircraft fuselages, to assist with meeting regulatory requirements on crashworthiness. To achieve certification, an equivalent level of occupant safety to that of previously certified, metallic fuselage transports has to be demonstrated in a "foreseeable survivable impact event", which is typically shown by combined test and analysis of fuselage section vertical drop tests with a range of impact velocities up to 30 ft./s (9.14 m/s) [3,4]. In a fuselage drop test, as illustrated in Fig. 1(a), energy is absorbed by irreversible damage of the lower structure (crumple zone), enhancing occupant safety. In wide-body, composite fuselage aircraft, such as the Airbus A350 XWB and the Boeing 787 Dreamliner, due to the relatively large height of the space below the cargo floor, it is possible to achieve the bulk of the energy absorption requirements via a sub-cargo structure involving crushable composite beams [3]. However, in single-aisle (i.e. narrow-body) aircraft, the height of the sub-cargo area is much less, so additional energy absorbing structures or devices will be required [1].

The German Aerospace Center (DLR) and Airbus have been working together for some time on novel, narrow-body composite fuselage designs, in which energy is absorbed via tensile- and bending-loaded energy-absorbing elements, in addition to more traditional compression-loaded elements [1]. As can be seen in Fig. 1(a), the fuselage typically deforms into a more oval shape during a crash, which loads some areas in tension, some in bending and others in compression. In Fig. 1(b) a concept is illustrated incorporating tensile, bending and compressive absorbers [1]. It has been predicted, via full-scale simulations, that more than 50% of the overall absorbed energy could be taken by the tension absorbers, so that much less energy would

* Corresponding author:
E-mail address: michael.mccarthy@ul.ie (M.A. McCarthy).

https://doi.org/10.1016/j.compstruct.2020.113327
Received 19 August 2020; Revised 12 October 2020; Accepted 9 November 2020
Available online 17 November 2020

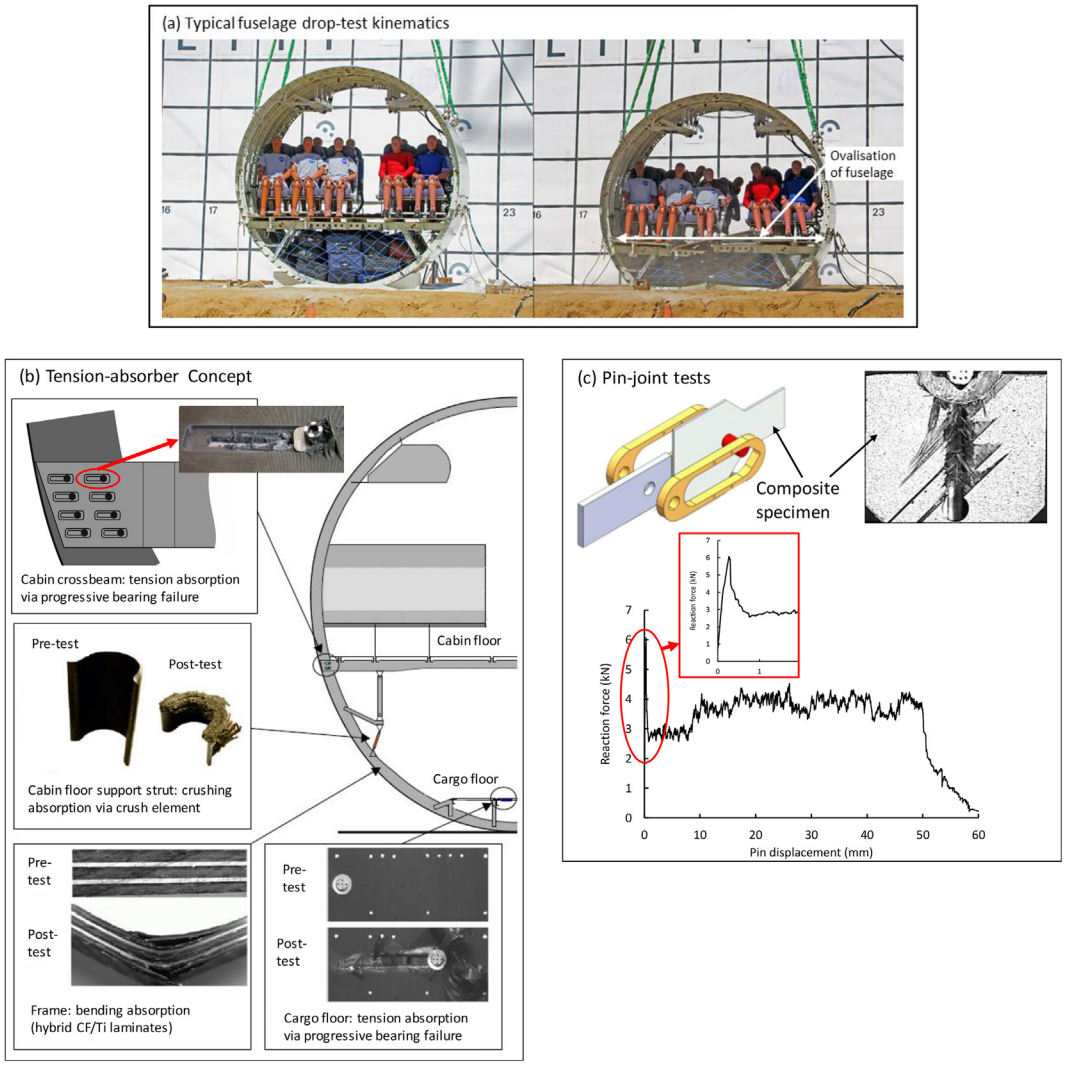

Fig. 1. (a) Typical fuselage test kinematics (adapted from [4]), (b) novel narrow-body composite fuselage concept incorporating tension-absorbing joint concept [1], (c) pin-joint tests for parameter studies [5].

need to be absorbed by the sub-cargo crush zone [1]. This has the added benefit of allowing a lighter cargo crossbeam. The focus of this paper is on the tension-absorber part of this design.

The DLR/Airbus "tension-absorber" joint concept, illustrated in Fig. 1(b), involves the modification of joints in areas such as the cargo and passenger cross-beams, which are loaded in tension as the fuselage deforms during impact. The modified joints would behave like normal joints under in-service loads, but in a crash would absorb considerable energy. The key design requirement is to prevent bolt pull-through or fracture during a crash, so that "extended bearing failure" occurs, resulting in the absorption of energy through crushing of the material in front of the bolt.

To examine individual material and geometric parameters, Airbus and DLR have studied a simplified version of the problem, namely a pin being pulled through a composite plate [2,6,7]. Recently [5,8], the current authors used this setup to study the effects of pin diameter (D) and laminate thickness (t) on bearing strength and specific energy absorption (SEA), for quasi-isotropic (QI) carbon/epoxy laminates, at quasi-static (QS) and dynamic (DY) loading rates, with results illustrated in Fig. 1(b). It was found that, provided a minimum thickness is used to avoid global bending, the SEA is strongly correlated with D/t ratio for both loading rates, with smaller values giving the best performance. Here, the optimal geometry from [5] is used to examine the effects of layup, stacking sequence and loading rate. As in [9], *layup* refers to the ply composition (percentage of plies in each direction), while *stacking sequence* refers to the location of each ply within the thickness.

While there have been several studies on the effects of loading rate [10–14], and stacking sequence [15–18], on composite bolted joint behaviour, they have mostly been focused on conventional joints. In such joints, while the initial failure may be in bearing, the ultimate failure is typically through bolt fracture, bolt pull-through, net-tension, shear-out or some combination thereof. Results depend on many variables, including joint type (single/double-lap), fastener type (protruding/countersunk head bolts, rivets), bolt diameter, laminate width and thickness, and so on. In general, conventional joints absorb relatively small amounts of energy, and joint strength and stiffness are the main interests in such studies.

Here, the focus is on the "extended bearing failure" mode that occurs in tension-absorber joints, Fig. 1(a), which is rarely seen in conventional joints. The main focus is on energy absorption, which is much higher than in conventional joints. On the other hand, the joints must also perform under in-service loads, so joint strength cannot be neglected. Relatively few authors have studied the behaviour of tension-absorber joints. Some have addressed single and multi-bolt versions [1,7,19] to assess design details like the bolt head and washer geometry, the machined slot to guide the bolt, and methods to prevent debris from blocking the bolt movement. For fundamental studies on

individual material or geometric parameters, a simplified pin-loaded setup like that in Fig. 1(b) has been used, since the effects of debris in the actual joint can be complex and unpredictable, and tend to mask the effects of the parameter of interest. Thus far, there have been two studies using the pin-loaded setup that addressed the loading rate. In [2], a range of different composite materials were examined at 200 mm/min (3.3×10^{-3} m/s) and 3 m/s, while in [14] a carbon/epoxy material with QI layup was tested at speeds ranging from 10^{-4} m/s to 1 m/s. In both studies, the load plateau after initial failure (and hence energy absorbed) decreased with increased loading rate, by amounts ranging from 20% to 60%, while in [14] the peak load increased with loading rate by about 20%. To date, there has been no systematic study of the effects of layup and stacking sequence under extended bearing failure.

There *have* been studies on stacking sequence effects in other energy-absorbing structures such as composite crush tubes [15,20–22]. Flat plates were examined in [23], and can be considered the equivalent of the current problem with an infinite bolt diameter. The energy-absorption process in [23] was quite similar to that found here and it was found that increasing the number of 0° plies and placing them in a block in the middle of the laminate, led to increased specific energy absorption. This finding has influenced the choice of stacking sequences here.

In the current work, the optimised geometry from our previous studies [5,8], consisting of a 4 mm diameter pin, and 2 mm thickness laminate, is used to study the effects of layup and stacking sequence at QS and 3 m/s loading speeds. Seven layups and 11 stacking sequences are tested, with key variables being the percentage of 0° plies, the position of the 0° plies within the laminate, and the changes in orientation at ply interfaces. Performance measures used are ultimate bearing strength (UBS), mass-specific energy absorption (SEA) and crush load efficiency (CLE). The chosen material is IM7/8552 carbon/epoxy, which has been used in the third world-wide composites failure exercise [24]. All parameters needed to calibrate damage and failure models for this material have been extensively characterised [25–27], so the results herein can be used for model validation without further testing. Three-dimensional computed tomography (3D CT) is used to examine damage progression in the QS tests.

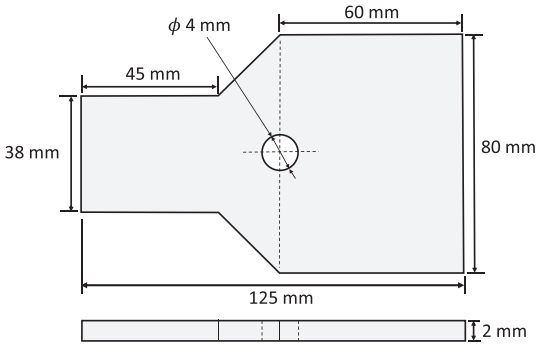

Fig. 2. Specimen dimensions.

2. Materials and methods

2.1. Specimen preparation and selection of stacking sequences

HexPly® IM7/8552 (EU version: 134 gsm) carbon fibre/epoxy composite pre-preg was obtained with a nominal ply thickness of 0.125 mm. Composite plates were laid up by hand, and autoclave-consolidated according to manufacturer instructions. Specimens with the geometry shown in Fig. 2 were extracted via waterjet cutting, and special tooling was procured to drill the holes with an H7 tolerance. The geometry was selected following a prior study [28], being narrow on one end to fit within the test machine grips, and wider on the other end to reduce edge effects as the pin moves through the laminate. Specimens had 16 plies, giving a nominal laminate thickness of 2 mm, and were tested with a 4 mm diameter pin.

The 11 stacking sequences are given in Table 1. The third column gives the layup, i.e. the percentage of plies in each direction, and there are seven in total. All stacking sequences are symmetric, and all but one (SS2) are balanced. SS3 – SS11 employ only 0°, 45°, −45° and 90° plies. The fourth column gives the maximum ply-to-ply change in orientation, while the fifth column gives the number of interfaces with a 90° change. In our previous study [5], on quasi-isotropic laminates, interfaces with a 45° change were found to be more resistant to delamination than those with a 90° change, due to lower interlaminar stresses. SS1 was chosen to test out the effect of having a *very* low maximum change in orientation (22.5°).

Besides the changes in ply orientation, the other two main variables are the percentage and position of 0° plies. As noted above, Hobbs and Adams [23] found for crushing of flat plates, that increasing the number of 0° plies, and placing them in a block in the middle of the lami-

Table 1

Code	Stacking sequence	Layup (ply composition)	Max ply-to-ply change	Number of 90° changes
SS1	$[-22.5 / -45 / -67.5 / 90 / 67.5 / 45 / 22.5 / 0]_s$	**[0°|22.5°|45°|67.5°|-67.5°|-45°|-22.5°|90°]** → [12.5%|12.5%|12.5%|12.5%|12.5%|12.5%|12.5%|12.5%]	22.5°	0
SS2	$[\pm 30 / -60 / 90 / 60 / 30 / 0_2]_s$	**[0°|30°|60°|-60°|-30°|90°]** → [25%|25%|12.5%|12.5%|12.5%|12.5%]	60°	0
SS3	$[45_2 / -45_2 / 90_2 / 0_2]_s$	**[0°|±45°|90°]** → [25% | 50% | 25%]	90°	4
SS4	$[45 / -45 / 90 / 0 / 45 / -45 / 90 / 0]_s$	**[0°|±45°|90°]** → [25% | 50% | 25%]	90°	8
SS5	$[45 / -45_2 / 90 / 45 / 0_3]_s$	**[0°|±45°|90°]** → [37.5% | 50% | 12.5%]	90°	2
SS6	$[45 / 90_2 / -45 / 0_4]_s$	**[0°|±45°|90°]** → [50% | 25% | 25%]	45°	0
SS7	$[45 / 0 / 90 / 0 / -45 / 0 / 90 / 0]_s$	**[0°|±45°|90°]** → [50% | 25% | 25%]	90°	8
SS8	$[90_2 / 45 / 0 / -45 / 0_3]_s$	**[0°|±45°|90°]** → [50% | 25% | 25%]	45°	0
SS9	$[45_2 / -45_2 / 0_4]_s$	**[0°|±45°|90°]** → [50% | 50% | 0%]	90°	2
SS10	$[45 / 90 / 0 / -45 / 0_4]_s$	**[0°|±45°|90°]** → [62.5% | 25% | 12.5%]	90°	2
SS11	$[45 / 0 / 90 / 0_2 / -45 / 0_2]_s$	**[0°|±45°|90°]** → [62.5% | 25% | 12.5%]	90°	4

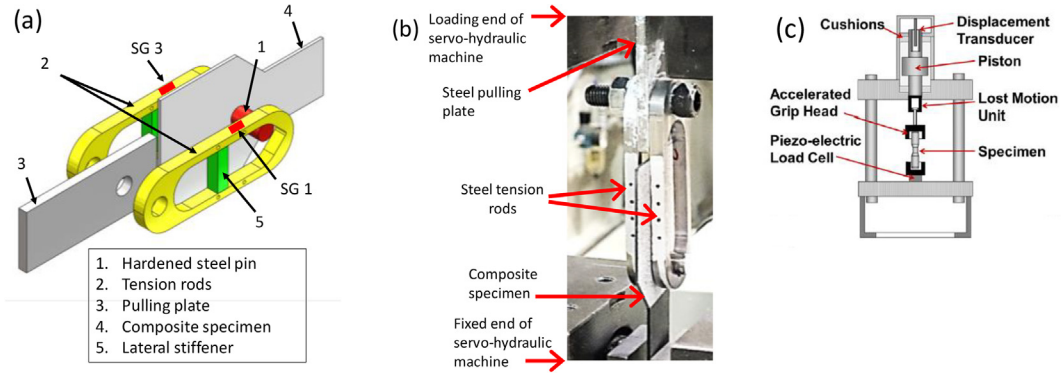

Fig. 3. (a) Exploded view of the test rig, (b) side view of the quasi-static test setup, (c) Zwick HTM 5020 servo-hydraulic dynamic test machine.

nate, led to increased SEA. Here, the percentage of 0° plies increases from 12.5% (SS1) to 25% (SS2, SS3, SS4), to 37.5% (SS5) to 50% (SS6, SS7, SS8, SS9) to 62.5% (SS10 and SS11). In SS3 the 0° plies are all located in the centre, while in SS4, they are not. The same applies to SS6 versus SS7/SS8 (these also differ in the maximum change in ply orientation), and to SS10 versus SS11. Finally, in SS2, the angle plies are chosen to be ±30° and ±60° rather than ±45°, and in SS9, the 90° plies are dispensed with. The energy absorbed by the 90° plies is through "tearing" rather than crushing (see [5]) so removing them is of interest to see the relative importance of tearing and crushing, even though doing so violates normal bolted joint design rules, leaving the joint susceptible to shear-out.

2.2. Experimental set-up

2.2.1. Quasi-static test set-up

A Zwick 100 kN servo-hydraulic test machine was used for the QS tests. A bespoke test rig, shown in Fig. 3(a), was designed to be low mass, with maximum visibility on the specimen. It contains three main components: a hardened steel pin, a pair of steel tensions rods used to load the pin, and a steel pulling plate bolted to the tension rods. As shown in Fig. 3(b), the pulling plate was gripped at the loading end of the test machine, and the composite specimen was gripped at the fixed end. The pulling plate was 6 mm thick, and by carefully centring the specimen between the tension rods, a 2 mm gap on each side of the specimen was provided for debris outflow. The test velocity was 10 mm/min and data from the piezoelectric 0–100 kN load cell was recorded at 10 Hz. Portemont et al. [14] showed for a similar pin-crushing problem that test speeds up to 60 mm/min cause no noticeable strain rate effects, so the velocity used here can be regarded as quasi-static. Identifiable black dots were marked on the pin for measurement of pin displacement using a JAI Inc. TM-2040GE CCD camera, and DIC software (DaVis, a product of LaVision GmbH). Three repeats were performed for each stacking sequence, with a fourth interrupted test performed for later 3D CT analysis.

2.2.2. Dynamic test set-up

A Zwick HTM 5020 servo-hydraulic machine, illustrated in Fig. 3 (c), was used for dynamic testing at 3 m/s. The 50 kN piezo-electric load cell outputs the load at 950 kHz and is capable of test speeds from 1 mm/s to 20 m/s. For tensile testing, the lost-motion adapter, which is attached to a free-piston, can accelerate up to the test speed without interacting with the specimen or grips. The pin displacement was determined using the same method as for the quasi-static tests, but using images taken at 30,000 frames per second with a high-speed FASTCAM SA-1.1 camera. Four repeats were performed for each stacking sequence.

For the dynamic tests, a lateral stiffener (item 5 in Fig. 3(a)), was added between the arms of each tension rod, to eliminate lateral vibration observed in pre-test videos. Even after making this modification, the load cell signal showed a significant level of oscillation, as can be seen for a sample test in Fig. 4. As is typical in dynamic tests [29–31], the load cell data shows clear evidence of system ringing at one particular frequency, throughout the entire test, which is caused by the impulse during load introduction that excites the test system. The usual strategy to mitigate this issue is to apply filtering, but results depend on the choice of filter, and care has to be taken not to compromise important characteristics in the signal. Here, a low pass filter with a cut-off frequency 4 kHz was used, which as can be seen in Fig. 4 is effective in reducing the contribution from system ringing, without greatly altering the average crushing load between 10 mm and 50 mm pin displacement, which is the key quantity determining energy absorption.

In the literature, it is suggested to attach strain gauges to the specimen near the grips [30] to obtain a signal less susceptible to ringing, but the specimen geometry in the present study did not allow enough space for this, see Fig. 2. As an alternative, four strain gauges were mounted on the sides of tension rods, two on each rod, as can be seen in Fig. 3(a). The data acquisition rate for the strain gauges was 500 kHz. The force obtained from an average of the gauge signals is also shown in Fig. 4. As can be seen, this signal is also unfortunately susceptible to significant oscillation, but once stable crushing is established (i.e. between 10 mm and 50 mm pin displacement), it matches well with the filtered load cell signal.

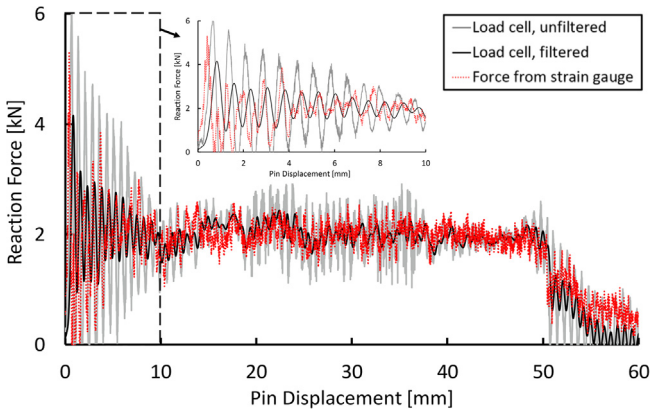

Fig. 4. Comparison of force signals obtained via different methods for SS_10_DY.

The most important quantity in this study is energy absorption, which is essentially the area under the force-deflection curve. It was found that this quantity varied very little whether the signal from the unfiltered load cell, the filtered load cell or the strain gauges was used. The other quantity of interest is the joint strength, which is based on the peak load. As can be seen from the inset to Fig. 4, which shows the first 10 mm of displacement, this quantity varies a lot depending on which signal is used (anything from 4 kN to 6 kN in the example shown). Which signal is "correct" is open to debate. In fact, the situation is even more complex than that shown here since sometimes the second or third peak in the strain gauge data was higher than the first. In the end, it was decided to use the filtered load cell signal for determination of joint strength as it was the most consistent among repeats. But it should be noted that the joint strength values reported for the dynamic tests have a lower confidence level than those for the quasi-static tests.

3. Results and discussions

3.1. Global response

Fig. 5 shows sample force-displacement responses for each stacking sequence at both loading rates. Each graph has an inset showing the QS response over the first 2 mm displacement. Later it will be shown

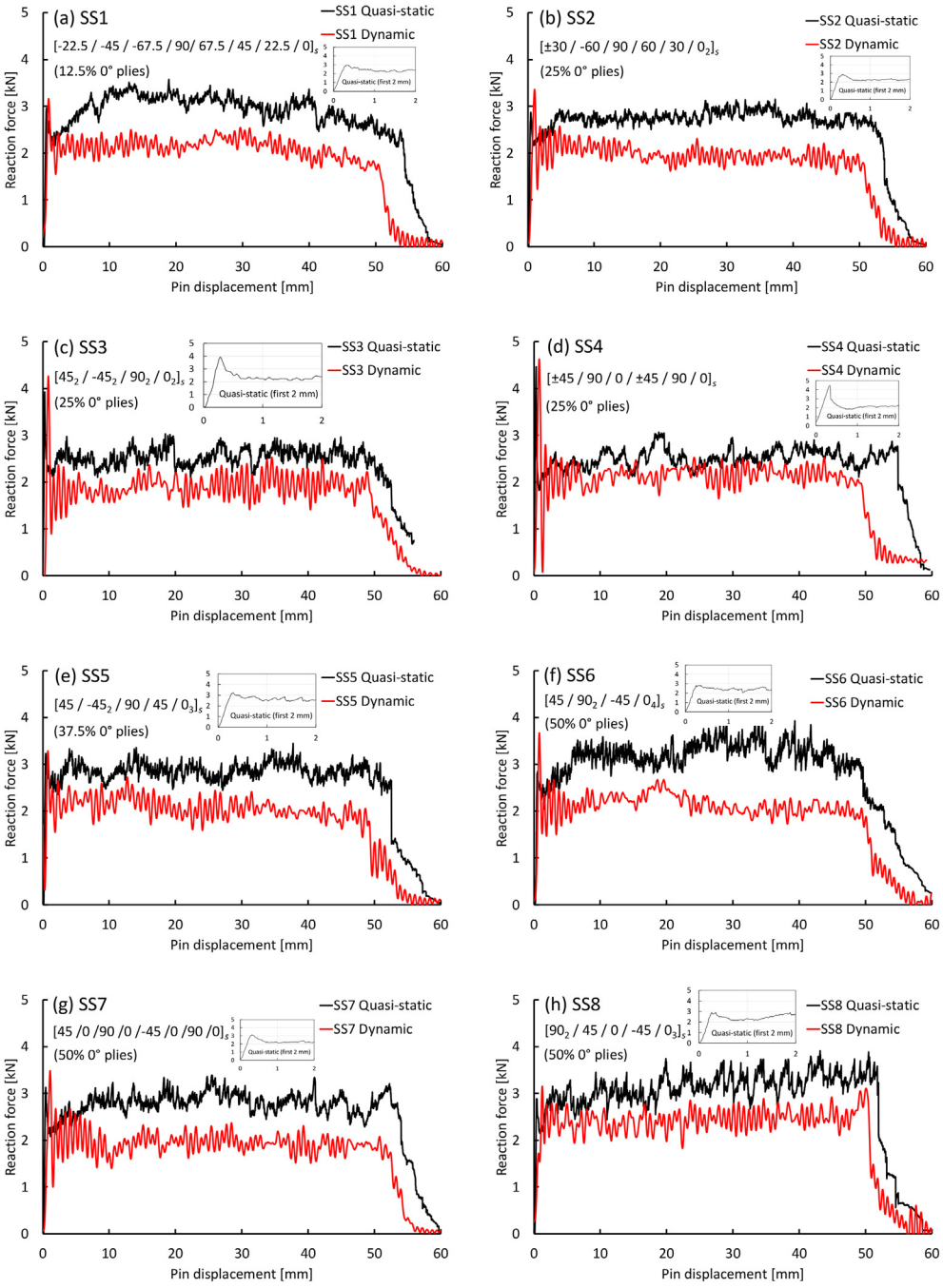

Fig. 5. Sample force-displacement response for each stacking sequence. Load is from load cell (filtered with cut-off frequency 4 kHz for dynamic data), displacement from DIC: Sample force-displacement response for each stacking sequence. Load is from load cell (filtered with cut-off frequency 4 kHz for dynamic data), displacement from DIC.

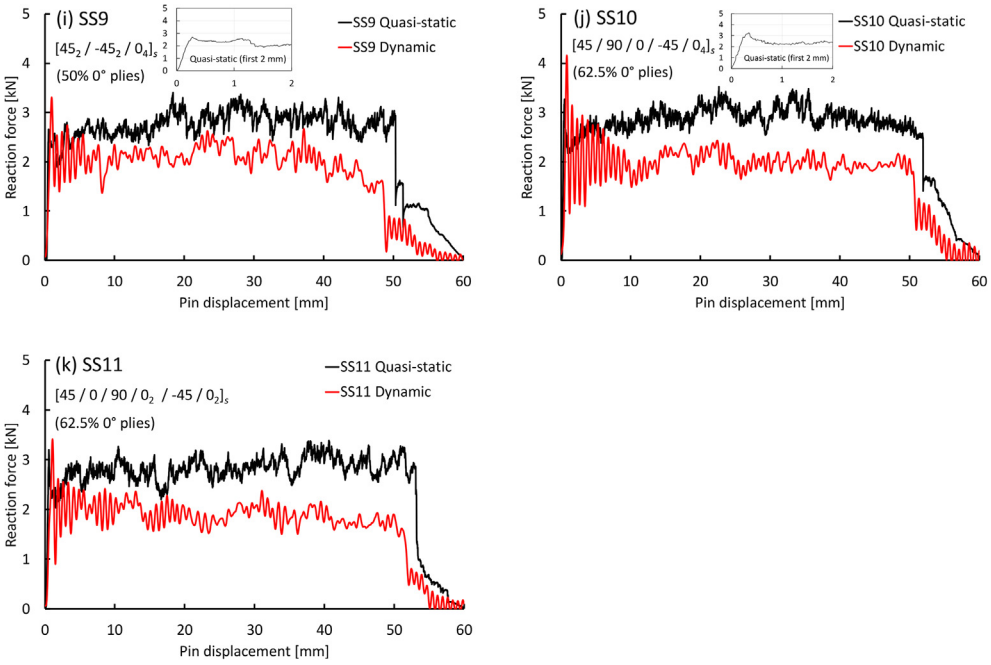

Fig. 5 (*continued*)

that the tests showed good repeatability with a low standard deviation for QS strength and energy absorption, and dynamic energy absorption. Only the dynamic strength showed a relatively high standard deviation, for the reasons outlined above.

Because of the very large w/d and e/d ratios (20 and 15 respectively), the initial failure mode is always bearing. At the end of the test, as the "effective" e/d ratio reduces, the final failure is by shear-out. Each force-displacement response thus has three main phases:

Phase 1: Linearly increasing load, with slight non-linearity (not visible at the scale shown) just prior to maximum load, F_{max}. For the QS tests (see insets) F_{max} occurred at about 0.3 mm displacement.

Phase 2: Sharp load drop, indicating "ultimate bearing failure", to a low value, which gradually transitions back up until a relatively stable crushing load, F_{crush}, is established at around 5 to 10 mm displacement. F_{crush} stays fairly constant until about 40 to 50 mm.

Phase 3: Load drop over the final 10–15 mm as the bolt pulls through the end of the laminate.

Consistently across all stacking sequences, it can be seen that as the loading rate increases from QS to 3 m/s, F_{max} increases, while F_{crush} (and hence energy absorption) decreases. The increase in $F_{\max}$ is attributed to the strain-rate dependent properties of IM7/8552. The maximum peak load is found for the QI SS4 layup (Fig. 5(d)) followed by SS3 and SS10. Whereas, the decrease in F_{crush} correlate with a decrease in width of damaged material and a decrease in debris in the bearing notch, under dynamic loading [8,14]. Maximum F_{crush} is displayed by SS6 and SS8, both of which have 50% 0° plies. The detailed description of the effect of loading rate on F_{max} and F_{crush} is given in a recently published study by the current authors [8].

To allow comparisons on a material level, the following performance parameters are defined. The UBS, σ_{ult}, is defined in accordance with ASTM standard D 5961/D 5961 M [32]:

$$\sigma_{ult} = \frac{F_{max}}{D \cdot t} \tag{1}$$

where D is the pin diameter and t is laminate thickness. The mass-specific energy absorption (SEA) is the integral of the force-deflection curve divided by the mass of destroyed material. For pin-crushing, it has been estimated [2], that for brittle fibre materials, the width of destroyed material is ~1.2D, so for comparison with that study, SEA is defined here as:

$$SEA = \frac{1}{m_{absorbed}} \int_0^{s_m} F \cdot ds = \frac{1}{1.2tDs_m} \int_0^{s_m} F \cdot ds \tag{2}$$

where ρ is material density and s_m is maximum pin displacement. s_m was taken as 40 mm, since the response beyond 40 mm showed significant variation (see Fig. 5). In reality, the width of destroyed material is difficult to define, as the damage spreads unevenly in each ply [5].

A summary of the findings from all tests for UBS is presented in Fig. 6, while SEA is shown in Fig. 7. Each value is an average from three tests for QS loading, and four tests for dynamic loading. Error bars indicate ± one standard deviation. Concerning UBS, Fig. 6, the standard deviation is low for QS tests (with the possible exception of SS4). In contrast, it is high for dynamic tests for the reasons indicated in Section 2.2.2. For SEA, Fig. 7, the standard deviation is low for both loading rates (actually lower for the dynamic tests).

For UBS, Fig. 6, the ranking between stacking sequences is fairly consistent between loading rates. For QS loading, SS1 and SS9 rank joint lowest. Their ranking is also low for dynamic loading, fifth lowest for SS1, third lowest for SS9. Overall, there is no discernible correlation between UBS and an increasing percentage of 0° plies. The UBS is highest for the QI layups, being highest for SS4, in which the plies of the same orientation are "dispersed" throughout the laminate, followed by SS3, in which plies of the same orientation are blocked together in pairs. This result holds at both QS and dynamic loading rates. For QS loading, the UBS is *substantially* (50–100 MPa) higher for QI layups than any of the other layups, which is an interesting and not necessarily intuitive result.

We examined the literature to see how this finding compared to previous work and were surprised at how few studies could be directly compared against. We focused only on pin-loaded examples with no lateral constraint. Collings [33], showed that adding up to 75% of ±45° to 0° layups or 90° layups increased bearing strength, but did not study QI layups. Wang et al. [34] and Park [17] showed that QI layups had higher bearing strength than 0/90 layups. Eriksson [35] and Hollmann [36] found that QI laminates had higher bearing strength than zero-dominated (60% 0°, 20% ±45°, 20% 90°) layups,

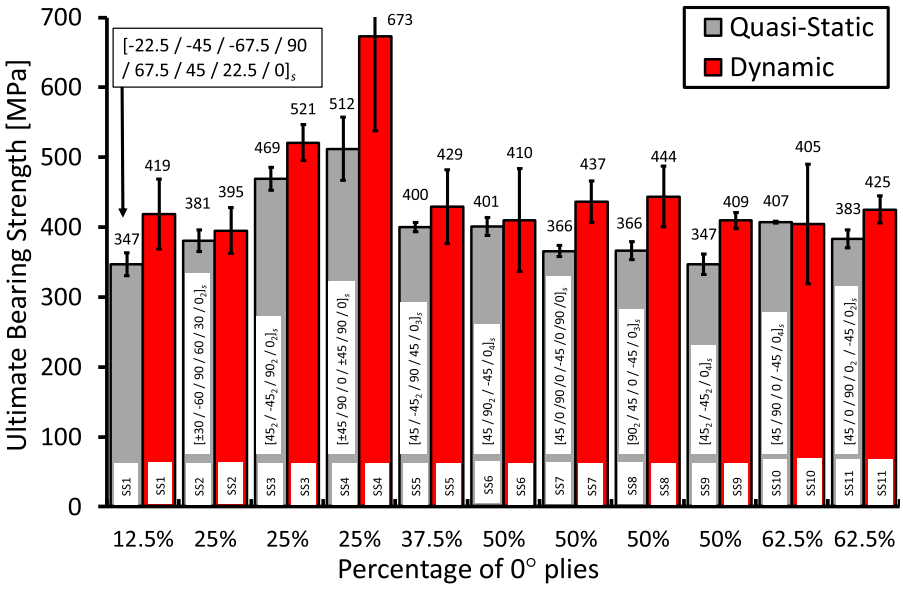

Fig. 6. Ultimate bearing strength (UBS) as a function of the stacking sequence.

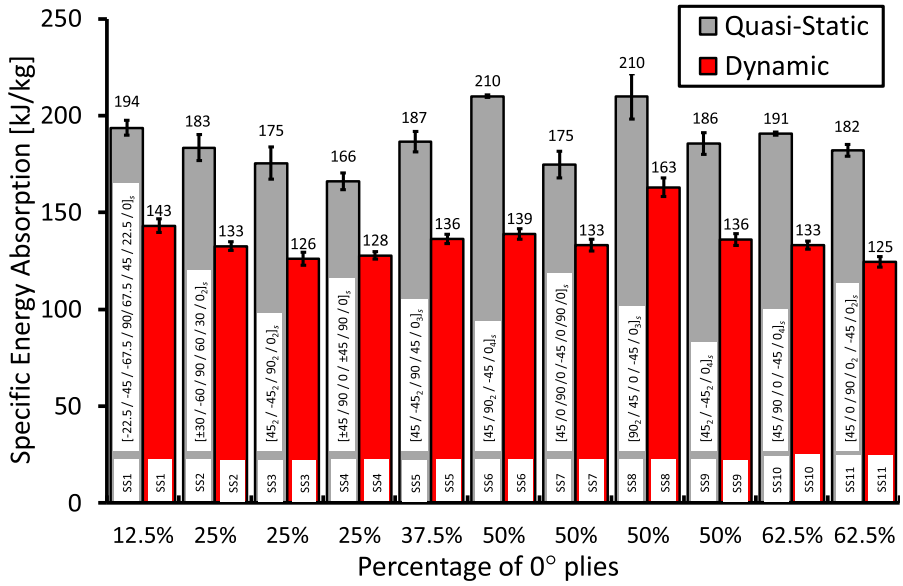

Fig. 7. Specific Energy absorption (SEA) as a function of the stacking sequence.

which agrees with our findings, but in both papers, some of that difference was due to the QI laminate having a lower D/t ratio than the zero-dominated laminate.

The most extensive studies on stacking sequence have been performed by industry, who tend not to reveal all test details. Hart-Smith in [37] shows a graph of bearing strength as a function of all possible combinations within the [0/±45/90] family of laminates. It shows QI layups to have the highest bearing strength, in agreement with our findings. But it also shows a plateau around the QI configuration indicating no significant reduction in bearing strength for "small" deviations from QI. This plateau includes three of our 50% 0° ply stacking sequences (SS6, SS7, and SS8), which contradicts our findings. However, even going back to the original Hart-Smith report, [38], it is not made clear which layups were actually tested to produce the plot in [37]. The most useful result we found was in a paper by Ireman et al. [39], which shows a "typical" design diagram used by Saab Military Aircraft. The diagram shows bearing strength for the [0/±45/90] family of laminates. A clear peak exists for a 0° content of 20–30%, with a reduction of 50–100 MPa for laminates with 40–50% 0° plies, more or less exactly in line with our findings. No details are given though for how the tests that resulted in this data were performed. Overall, as far as we could determine, our results for bearing strength as a function of stacking sequence (with all other variables held fixed) are the most comprehensive to date in the open literature and are not contradicted by previous findings.

The reason why UBS is maximum for QI layups may be as follows. Bearing failure in a pin-loaded joint occurs when the material in front of the hole buckles due to sudden delamination and "brooming" of the outer plies, as well as fibre-kinking and breakage. In this sense, it is similar to the initial failure process when crushing flat plates. How-

ever, differently from flat plates, only the material in front of the hole buckles, and this material is *supported* against bucking by the non-failing material on either side. Thus, the resistance to bearing failure depends not only on the compressive properties of the material that buckles, but also on the tensile and shear properties of the material either side of the hole that supports the material that will buckle. Thus, the combination of tensile, compressive and shear strength provided by a QI layup may be the reason why it gives the best bearing strength. In future work, we will explore this theory via modelling.

Turning to SEA, Fig. 7, two of the 50% 0° ply laminates rank highly. SS6 and SS8 rank joint 1st under QS loading, while at 3 m/s, SS8 ranks 1st and SS6 ranks 3rd. In contrast, SS7 and SS9, which also have 50% 0° plies, rank 10th/6th and 6th/5th respectively, under QS/dynamic loading. Interestingly, the maximum change in ply orientation is just 45° for both SS6 and SS8 (see Table 1), whereas, for SS7 and SS9, there are 90° changes (with SS7 having the most such changes – eight – and the lowest SEA of the four). It seems that having more 0° plies, up to a limit of about 50% can be advantageous, but resistance to delamination is very important too.

This latter point is strongly reinforced by the surprising performance of SS1, which with just 12.5% 0° plies, ranks 3rd/2nd in SEA under static/dynamic loading. SS1 has the lowest maximum change in ply orientation (22.5°) so should have a strong resistance to delamination. This will be examined further in the next section. Finally, it is noticeable, at least to some extent, that an inverse relationship exists between UBS ranking and SEA ranking. For example, SS4 ranks 1st/1st for UBS at static/dynamic loading but only 11th/9th for SEA. SS3 ranks 2nd/2nd for UBS but 9th/10th for SEA. Conversely, SS1 ranks 11th/7th for UBS but 3rd/2nd for SEA. A similar comment applies to SS6.

A quantity often used to rank energy absorption devices is the crush load efficiency (CLE). Taking F_{crush} as the mean load over 10–40 mm displacement, CLE is defined here as:

$$CLE = \frac{F_{crush}}{F_{max}} \tag{3}$$

A high CLE indicates high energy absorption, with a low peak load, which is desirable to limit injuries. Fig. 8 shows the CLE for the various stacking sequences. SS6 and SS8 rank best overall at both loading rates. SS1 ranks a close 3rd under quasi-static loading, but drops somewhat under dynamic loading, due to a high dynamic UBS. The dynamic standard deviations are high due to the high uncertainty in dynamic UBS. At the bottom comes SS4, which apparently is an excellent choice for in-service loads, but not for energy absorption.

3.2. Local behaviour

To gain some further insight, QS tests were performed on all stacking sequences, up to a pin displacement of 0.75 mm. This is about 0.4–0.5 mm beyond the occurrence of peak load, F_{max}, as can be seen from Fig. 5. Each specimen was then scanned in a Zeiss Xradia 500 Versa, 3D CT, X-ray microscope (Carl Zeiss X-ray Microscopy, Pleasanton, CA, USA). The field of view was 15 × 15 mm^2 and the voxel size was 15 × 15 × 15 μm^3. Videos showing all cross-sections from each specimen are included in the supplementary information. Here, the bearing plane (the plane directly in front of the pin) is chosen to illustrate the key differences between the stacking sequences, see Fig. 9. For each case, the stacking sequence, UBS (QS and dynamic), SEA (QS and dynamic), corresponding rankings (1 to 11), the percentage of 0° plies, maximum orientation change, and the number of 90° interface changes are included for convenience. As shown in the first row, colour code is used to illustrate ply orientations in SS3 – SS11, a blue horizontal line highlights 90° changes in the figures, while a red slash highlights them in the stacking sequence text. A vertical dashed line is shown at a distance of one thickness (i.e. 2 mm) from the hole edge. Plies in the laminate centre that are still essentially perpendicular to the pin at this location, and thus providing strong resistance to pin movement, as well as lateral support to the other plies will be referred to as "intact" and are shown in black lettering. Plies that have bent away from the load direction are assumed to provide much less resistance to pin movement and minimal lateral support and are indicated with red lettering.

The importance of having low ply-to-ply changes in orientation for high SEA becomes very clear from Fig. 9. The top-ranked stacking sequences, SS1, SS6 and SS8 show high resistance to delamination and, as a result, have a thick central block of "intact" plies with high structural integrity at 2 mm from the hole edge. SS1, Fig. 9(a), has a central block of 12 plies with no delaminations. SS6, Fig. 9(f), has a central block of 14 plies. Although there is a delamination within this block, the smaller block has not split away and is still providing significant resistance to pin movement and lateral support to the larger block. In SS8, there are three blocks of 4, 8 and 4 plies, but none of

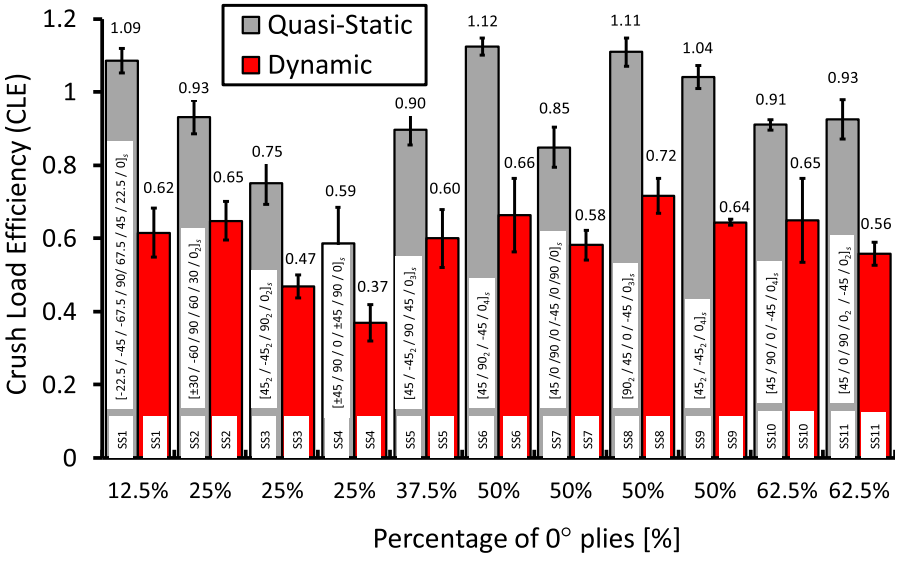

Fig. 8. Crush load efficiency, F_{max}/F_{crush}.

them has split away significantly, so all 16 plies are providing strong resistance to pin movement, and lateral support to each other. SS1, SS6 and SS8 have no 90° changes in orientation, and the maximum change in orientation is just 22.5° in SS1 and 45° in SS6 and SS8.

In contrast, stacking sequences with a large number of 90° changes in orientation have poor SEA. SS4 and SS7 have eight 90° changes and rank 11th/9th and 10th/(Joint 6th) under quasi-static/dynamic loading respectively. The reason why can be seen in Fig. 9. SS4 and SS7 both have a large number of delaminations, with a central "intact" block of just nine and seven plies respectively at 2 mm from the hole edge. For SS4 even the block of nine has a delamination within it. SS11, with four 90° changes in orientation, also has a lot of delaminations and has a SEA ranking of 8th/11th. While 12 plies are indicated as "intact" for SS11, Fig. 9(k), there are 4–5 delaminations within this central block, so its structural integrity is poor.

Other stacking sequences with an intermediate number of 90° changes have an intermediate SEA ranking. In fact, if the stacking sequences are ordered by the number of 90° changes, and then by the maximum change, see Table 2, we find a very good correlation with SEA (4th column). The only real outlier is SS2. Like SS1, it has no 90° changes, but its maximum ply-to-ply change is 60° instead of 22.5°. Like SS1, it shows good delamination resistance, Fig. 9(b), but the delaminations between plies 2 and 3, and plies 14 and 15 extend considerably further than for SS1, leading to a thinner block of intact plies between 2 mm and 4 mm from the hole edge, and hence lower resistance to pin movement. Overall, while the number of 0° plies influences SEA, the more important variable seems to be the change in orientation at ply interfaces.

Also shown in Table 2 is QS UBS. Dynamic UBS is not shown due to the lower confidence level in those results. Here, the correlation with

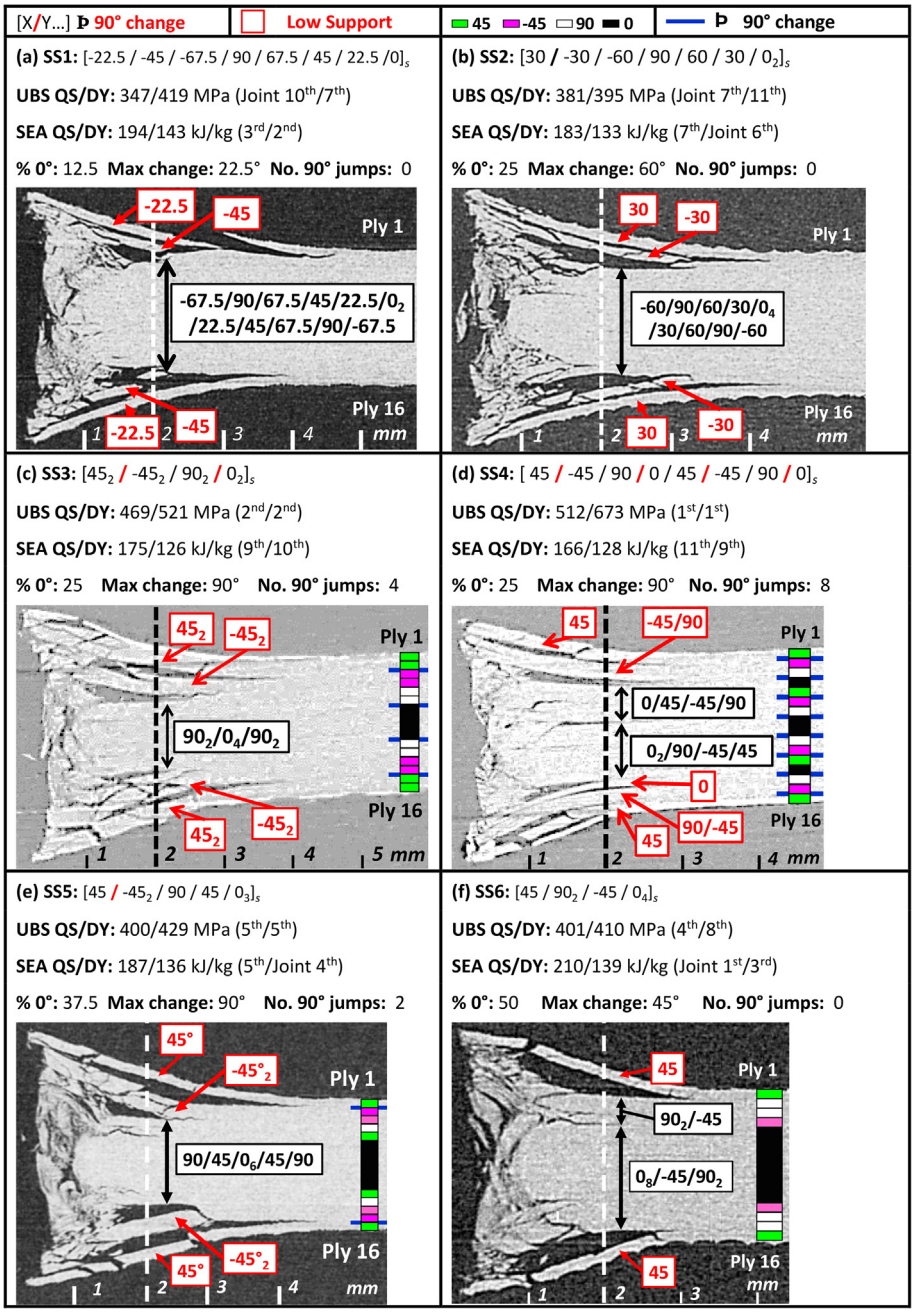

Fig. 9. CT images at the bearing plane, at a pin displacement of 0.75 mm CT images at the bearing plane, at a pin displacement of 0.75 mm.

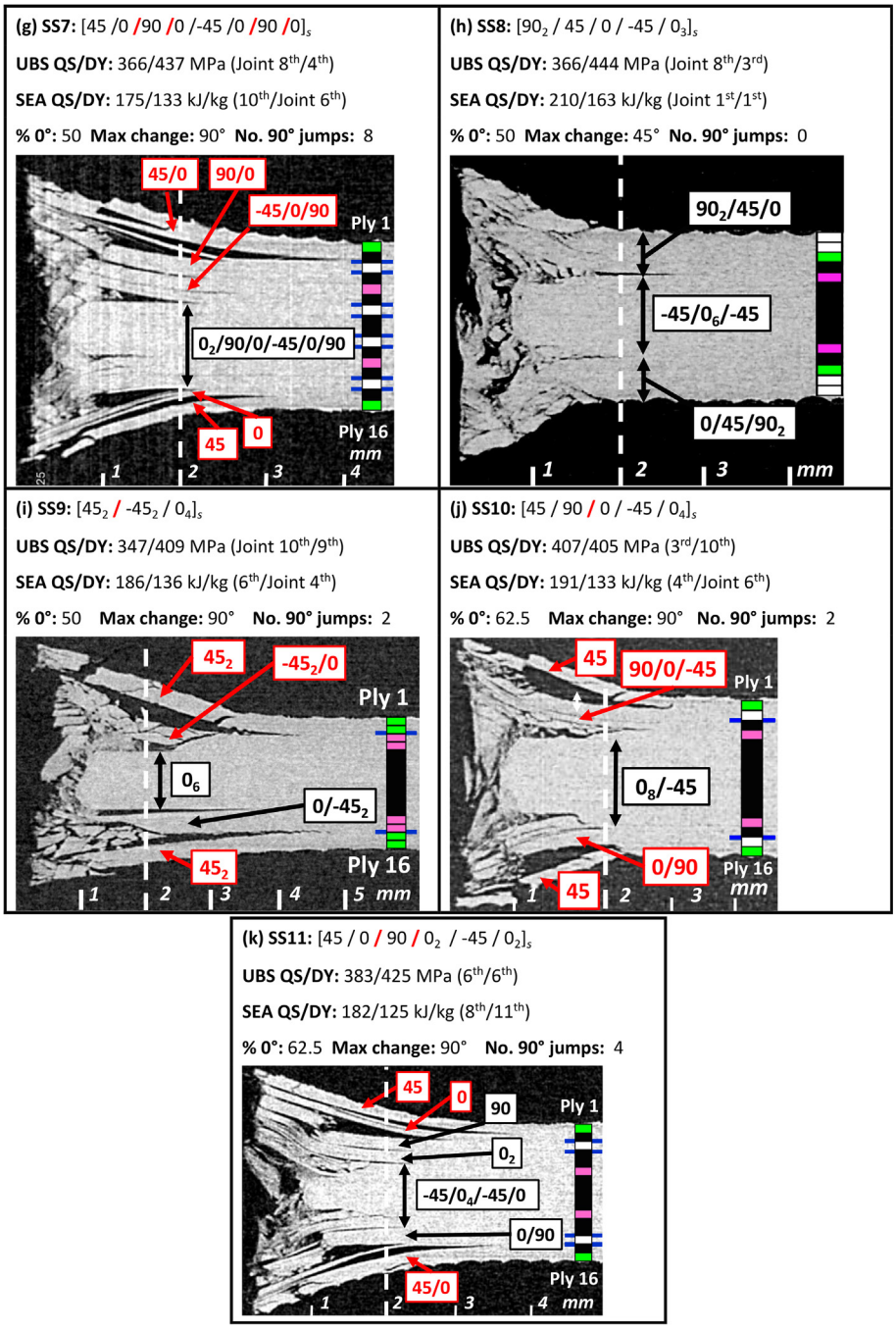

Fig. 9 (*continued*)

Table 2
SEA for stacking sequences ordered by number of 90° changes, then maximum ply-to-ply change.

Code	Number of 90° changes	Max ply-to-ply change	SEA rank (QS/DY)	QS UBS rank
SS1	0	22.5°	3rd/2nd	Joint 10th
SS8	0	45°	(Joint 1st)/1st	Joint 8th
SS6	0	45°	(Joint 1st)/3rd	4th
SS2	0	60°	7th/6th	7th
SS5	2	90°	5th/(Joint 4th)	5th
SS9	2	90°	6th/(Joint 4th)	Joint 10th
SS10	2	90°	4th/(Joint 6th)	3rd
SS3	4	90°	9th/10th	2nd
SS11	4	90°	8th/11th	6th
SS7	8	90°	10th/(Joint 6th)	Joint 8th
SS4	8	90°	11th/9th	1st

the number of 90° changes is not as good. As noted before, QI laminates had the highest UBS, with SS4 highest of all, which may be partially due to a large number of delaminations, Fig. 9(d). In order for bearing failure to occur, it may be that all these delaminations have to propagate suddenly together, leading to a higher UBS than SS3. Table 2 allows a designer to choose a stacking sequence for optimum energy absorption, optimum strength, or an optimum compromise between the two.

4. Conclusions

An experimental study has been performed on the energy absorption characteristics of pin-loaded laminates at quasi-static and dynamic loading rates. Seven layups and 11 stacking sequences were tested, with key variables being the percentage of 0° plies (from 12.5% to 62.5%), the position of the 0° plies, and the changes in orientation at ply interfaces. The following are the main conclusions:

I. The key to high SEA seems to be to maintain a thick central block of largely undelaminated plies, about one thickness from the hole edge. A very much secondary aim is to have as many 0° plies as possible within this block.
II. To achieve this, the most important parameter is the change in orientation at ply interfaces. Laminates with a maximum change of 45° or less performed best. For laminates which had at least one 90° change, the ones with fewer 90° changes performed best. The percentage of 0° plies was much less important. One of the best-performing laminates had only 12.5% 0° plies.
III. The above findings were true at quasi-static and 3 m/s loading rates.
IV. As the loading rate increased, SEA decreased, and ultimate bearing strength (UBS) increased. It should be noted though that the dynamic UBS values have a lower confidence level than the other results.
V. UBS was highest for QI laminates. This appears to be in line with previous results but is the most comprehensive exposition of this result to date, as far as we could tell. Among QI laminates, ones with no blocking of plies had the highest UBS. This is likely to be related to a large number of delaminations displayed by this stacking sequence.
VI. The laminate displaying the overall highest crush load efficiency at both loading rates (about 1.1 at QS and 0.72 at dynamic rates) was SS8 which had 50% 0° plies ($[90_2/45/0/-45/0_3]_s$). However, SS6 and SS1 (with 12.5% 0° plies) were not far behind.

Because IM7/8552 has been widely characterised in the literature, the findings can be used to test out composites damage models. In a future paper, results from a three-dimensional finite element model using our own damage model will be presented.

CRediT authorship contribution statement

Jazib Hassan: Conceptualization, Methodology, Investigation, Validation, Writing-Original draft preparation, Data Curation, Visualisation, Formal analysis. **Ronan O'Higgins:** Supervision, Writing-Review & Editing. **Thomas Feser:** Conceptualization, Methodology. **Matthias Waimer:** Conceptualization, Methodology, Supervision. **Conor McCarthy:** Supervision, Funding acquisition. **Nathalie Toso:** Funding acquisition, Project administration. **Michael McCarthy:** Conceptualization, Methodology, Supervision, Funding acquisition, Writing-Review & Editing, Resources, Visualisation, Project administration, Formal Analysis, Data Curation.

Declaration of competing interest

The authors declare that they have no known competing financial interests or personal relationships that could have appeared to influence the work reported in this paper.

Acknowledgements

This work was supported by EU Horizon 2020 Marie Skłodowska-Curie Actions Innovative Training Network - ICONIC [grant agreement: 721256]. The authors would like to thank Michael E. Byrne from the University of Limerick for performing the CT scans.

Data availability

The raw/processed data required to reproduce these findings cannot be shared at this time as the data also forms part of an ongoing study.

Appendix A. Supplementary data

CT scan videos generated with Dragonfly 4.1 for Windows 10 [40] are included in the supplementary data. They show all slices of the interrupted test specimens. Supplementary data to this article can be found online at https://doi.org/10.1016/j.compstruct.2020.113327.

References

[1] Waimer M, Feser T, Schatrow P, Schueler D. Crash concepts for CFRP transport aircraft – comparison of the traditional bend frame concept versus the developments in a tension absorbers concept. International Journal of Crashworthiness 2018;23:193–218.
[2] Heimbs S, Bergmann T. Bearing mode absorber – on the energy absorption capability of pulling a bolt through a composite or sandwich plate. Procedia Engineering 2014;88:149–56.
[4] Bolukbasi AO, Baxter TR, Nguyen TA, Rassaian M, Davis KR, Koch W, et al. Energy-absorbing floor structure for fuselage of aircraft e.g. civilian or military aircraft, includes coupling units which fix structural members to fuselage frame, floor beam, and support piece. In: Boeing Co, US Patent Number 8376275-B2.
[4] Littell JD. A summary of results from two full-scale Fokker F28 fuselage section drop tests. In: NASA TM–2018-219829.
[5] Hassan J, Feser T, O'Higgins RM, Waimer M, McCarthy CT, Toso N, et al. Energy absorption capability of composite bolted joints undergoing extended bearing failure. Composite Structures 2020;237:111868.
[8] Bergmann T. Beitrag zur Charakterisierung und Auslegung zugbelasteter Energieabsorberkonzepte mittels experimenteller, analytischer und numerischer Methoden. Kaiserslautern, Germany: TU Kaiserslautern; 2016.
[7] Feser T, Waimer M. Numerical simulation of progressive bearing failure of bolted joints in CFRP aircraft structures. In: First international conference on impact loading of structures and materials. Turin, Italy.
[8] Feser T, Hassan J, Waimer M, O'Higgins RM, McCarthy CT, Toso N, et al. Effects of transient dynamic loading on the energy absorption capability of composite bolted joints undergoing extended bearing failure. Composite Structures 2020;247:112476.
[9] Daniel IM, Ishai O. Engineering mechanics of composite materials. 2nd ed. 198 Madison Avenue, New York, New York 10016: Oxford University Press, Inc.; 2006.
[10] Heimbs S, Schmeer S, Blaurock J, Steeger S. Static and dynamic failure behaviour of bolted joints in carbon fibre composites. Composites Part a-Applied Science and Manufacturing 2013;47:91–101.
[11] Pearce GMK, Johnson AF, Heiner AK, Thomson RS. A study of dynamic pull-through failure of composite bolted joints using the stacked-shell finite element approach. Composite Structures. 2014;118:86–93.
[12] Egan B, McCarthy CT, McCarthy MA, Gray PJ, O'Higgins RM. Static and high-rate loading of single and multi-bolt carbon–epoxy aircraft fuselage joints. Compos A: Appl Sci Manuf 2013;53:97–108.
[13] Li QM, Mines RAW, Birch RS. Static and dynamic behaviour of composite riveted joints in tension. International Journal of Mechanical Sciences 2001;43:1591–610.
[14] Portemont G, Berthe J, Deudon A, Irisarri FX. Static and dynamic bearing failure of carbon/epoxy composite joints. Composite Structures. 2018;204:131–41.
[15] Riccio A, Mozzillo G, Scaramuzzino F. Stacking sequence effects on fatigue intra-laminar damage progression in composite joints. Applied Composite Materials 2013;20:249–73.
[16] Aktas A, Dirikolu MH. The effect of stacking sequence of carbon epoxy composite laminates on pinned-joint strength. Composite Structures. 2003;62:107–11.
[17] Park H-J. Effects of stacking sequence and clamping force on the bearing strengths of mechanically fastened joints in composite laminates. Composite Structures. 2001;53:213–21.

[18] McCarthy MA, Lawlor VP, Stanley WF, McCarthy CT. Bolt-hole clearance effects and strength criteria in single-bolt, single-lap, composite bolted joints. Composites Science and Technology 2002;62:1415–31.
[19] Schatrow P, Waimer M. Crash concept for composite transport aircraft using mainly tensile and compressive absorption mechanisms. CEAS Aeronautical Journal 2016;7:471–82.
[20] Jiang H, Ren Y, Gao B, Xiang J. Numerical investigation on links between the stacking sequence and energy absorption characteristics of fabric and unidirectional composite sinusoidal plate. Composite Structures. 2017;171:382–402.
[21] Farley GL, Jones RM. Crushing characteristics of continuous fiber-reinforced composite tubes. Journal of Composite Materials. 1992;26:37–50.
[22] Mahdi E, Hamouda AMS, Sebaey TA. The effect of fiber orientation on the energy absorption capability of axially crushed composite tubes. Materials & Design (1980–2015) 2014;56:923–8.
[23] Hobbs JM, Adams DO. Laminate design for crashworthiness of carbon/epoxy composites. In: Aerospace Structural Impact Dynamics International Conference (ASIDIC 2015). Seville, Spain.
[24] Kaddour AS, Hinton MJ, Smith PA, Li S. The background to the third world-wide failure exercise. Journal of Composite Materials 2013;47:2417–26.
[25] Koerber H, Camanho PP. High strain rate characterisation of unidirectional carbon-epoxy IM7-8552 in longitudinal compression. Composites Part a-Applied Science and Manufacturing 2011;42:462–70.
[26] Kuhn P, Catalanotti G, Xavier J, Camanho PP, Koerber H. Fracture toughness and crack resistance curves for fiber compressive failure mode in polymer composites under high rate loading. Composite Structures 2017;182:164–75.
[27] Cui H, Thomson D, Pellegrino A, Wiegand J, Petrinic N. Effect of strain rate and fibre rotation on the in-plane shear response of $\pm 45^{\circ}$ laminates in tension and compression tests. Composites Science and Technology 2016;135:106–15.
[28] Hassan J, O'Higgins RM, Feser T, McCarthy CT, Waimer M, Toso N, et al. Investigation of geometrical and composite material parameters for tension-absorbing bolted joints. In: Twenty-second international conference on composite materials (ICCM22). Melbourne, Australia.
[29] Yang X, Hector LG, Wang J. A combined theoretical/experimental approach for reducing ringing artifacts in low dynamic testing with servo-hydraulic load frames. Experimental Mechanics 2014;54:775–89.
[30] Xiao X. Dynamic tensile testing of plastic materials. Polymer Testing 2008;27:164–78.
[31] Xia Y, Zhu J, Wang K, Zhou Q. Design and verification of a strain gauge based load sensor for medium-speed dynamic tests with a hydraulic test machine. International Journal of Impact Engineering 2016;88:139–52.
[32] ASTM D5961/D5961M-17. Standard test method for bearing response of polymer matrix composite laminates. West Conshohocken, PA: ASTM International; 2017.
[33] Collings TA. On the bearing strengths of CFRP laminates. Composites 1982;13:241–52.
[34] Wang H-S, Hung C-L, Chang F-K. Bearing failure of bolted composite joints. Part I: experimental characterization. Journal of Composite Materials 1996;30:1284–313.
[35] Eriksson I. On the bearing strength of bolted graphite epoxy laminates. Journal of Composite Materials. 1990;24:1246–69.
[36] Hollmann K. Failure analysis of bolted composite joints exhibiting in-plane failure modes. Journal of Composite Materials. 1996;30:358–83.
[37] Hart-Smith LJ. Design and analysis of bolted and riveted joints in fibrous composite structures. Recent Advances in Structural Joints and Repairs for Composite Materials 2003:211–54.
[38] Hart-Smith LJ. Bolted joints in graphite-epoxy composites. National Aeronautics and Space Administration, Washington D.C. 20546: Douglas Aircraft Company; 1976. p. 1–156.
[39] Ireman T, Nyman T, Hellbom K. On design methods for bolted joints in composite aircraft structures. Composite Structures. 1993;25:567–78.
[40] Dragonfly 4.1. Montreal, Canada: Object Research Systems (ORS) Inc; 2018.